Article

Cell Reports

MECP2 Is Post-transcriptionally Regulated during Human Neurodevelopment by Combinatorial Action of RNA-Binding Proteins and miRNAs

Graphical Abstract

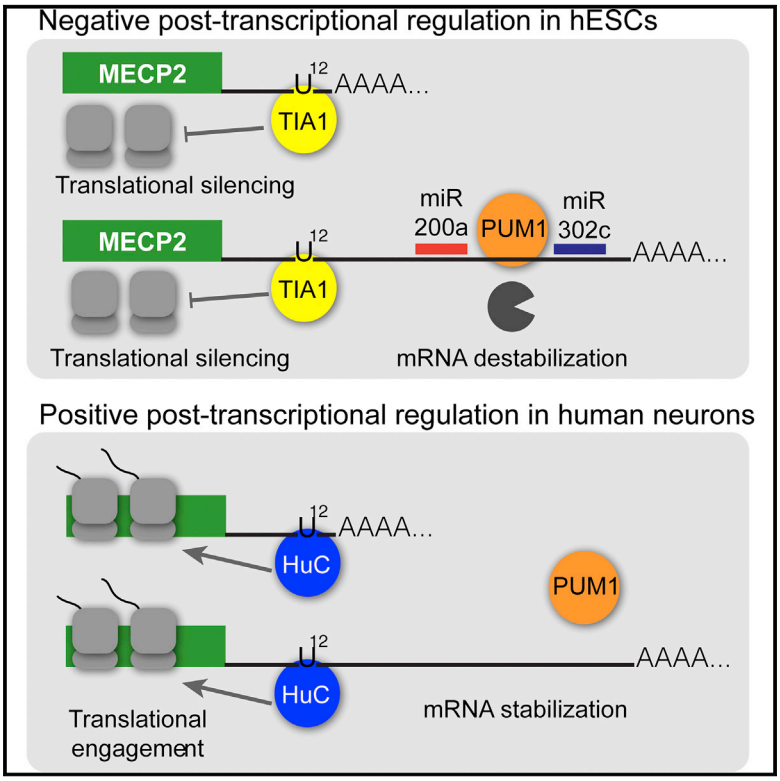

Highlights

- hESC model to study neurodevelopmental regulation of *MECP2* 3′ UTR use and function
- *MECP2* long 3′ UTR transcript is destabilized by PUM1 and miRNAs in hESCs
- MECP2 translation is repressed by TIA1 in hESCs and enhanced by HuC in neurons
- Combinatorial circuitry regulates *MECP2* 3′ UTR stability and MECP2 protein levels

Authors

Deivid C. Rodrigues, Dae-Sung Kim, Guang Yang, ..., Benjamin J. Blencowe, Quaid Morris, James Ellis

Correspondence

jellis@sickkids.ca

In Brief

Precise control of MECP2 protein levels is required for normal neurological function. Rodrigues et al. use hESCs to model neurodevelopment, and they demonstrate that combinatorial post-transcriptional circuitry, involving differential regulation of mRNA stabilization and translation efficiency in stem cells and neurons, controls *MECP2* 3′ UTR length and accumulation of MECP2 protein levels.

Rodrigues et al., 2016, Cell Reports *17*, 720–734
October 11, 2016
http://dx.doi.org/10.1016/j.celrep.2016.09.049

CellPress

OPEN ACCESS
CellPress

Cell Reports
Article

MECP2 Is Post-transcriptionally Regulated during Human Neurodevelopment by Combinatorial Action of RNA-Binding Proteins and miRNAs

Deivid C. Rodrigues,[1] Dae-Sung Kim,[1,5] Guang Yang,[2] Kirill Zaslavsky,[1,3] Kevin C.H. Ha,[3,4] Rebecca S.F. Mok,[1,3] P. Joel Ross,[1,6] Melody Zhao,[1,3] Alina Piekna,[1] Wei Wei,[1] Benjamin J. Blencowe,[3,4] Quaid Morris,[3,4] and James Ellis[1,3,7,*]
[1]Program in Developmental & Stem Cell Biology, The Hospital for Sick Children, Toronto, ON M5G0A4, Canada
[2]Program in Neurosciences & Mental Health, The Hospital for Sick Children, Toronto, ON M5G0A4, Canada
[3]Department of Molecular Genetics, University of Toronto, Toronto, ON M5S1A8, Canada
[4]Donnelly Center for Cellular and Biomolecular Research, University of Toronto, Toronto, ON M5S3E1, Canada
[5]Present address: Department of Biotechnology, Korea University Seoul, Seoul 02841, Korea
[6]Present address: Department of Biology, University of Prince Edward Island, Charlottetown, PE C1A4P3, Canada
[7]Lead Contact
*Correspondence: jellis@sickkids.ca
http://dx.doi.org/10.1016/j.celrep.2016.09.049

SUMMARY

A progressive increase in MECP2 protein levels is a crucial and precisely regulated event during neurodevelopment, but the underlying mechanism is unclear. We report that *MECP2* is regulated post-transcriptionally during in vitro differentiation of human embryonic stem cells (hESCs) into cortical neurons. Using reporters to identify functional RNA sequences in the *MECP2* 3′ UTR and genetic manipulations to explore the role of interacting factors on endogenous *MECP2*, we discover combinatorial mechanisms that regulate RNA stability and translation. The RNA-binding protein PUM1 and pluripotent-specific microRNAs destabilize the long *MECP2* 3′ UTR in hESCs. Hence, the 3′ UTR appears to lengthen during differentiation as the long isoform becomes stable in neurons. Meanwhile, translation of *MECP2* is repressed by TIA1 in hESCs until HuC predominates in neurons, resulting in a switch to translational enhancement. Ultimately, 3′ UTR-directed translational fine-tuning differentially modulates MECP2 protein in the two cell types to levels appropriate for normal neurodevelopment.

INTRODUCTION

Methyl CpG-binding protein 2 (*MECP2*) modulates global transcription and translation that is crucial for normal brain development and physiology (Li et al., 2013; Lyst and Bird, 2015). Heterozygous mutations of the *MECP2* gene cause Rett syndrome, and mild overexpression in mice or duplications and triplications in the *MECP2* locus in humans lead to neurological impairment (Chahrour and Zoghbi, 2007). These studies suggest that MECP2 protein levels must be tightly regulated during neurodevelopment in order to maintain proper regulation of a large number of genes.

MECP2 protein levels correlate poorly with mRNA levels in different tissues, suggesting important roles for post-transcriptional mechanisms (Pelka et al., 2005; Shahbazian et al., 2002). Although specific microRNAs (miRNAs) are known to repress *MECP2* in the fetal brain (Han et al., 2013) and primary cortical neurons (Klein et al., 2007), the pathways that post-transcriptionally downregulate *MECP2* in pluripotent stem cells and upregulate in neurons are unknown. Moreover, the physiological significance of premature MECP2 protein overexpression in pluripotent cells is untested. *MECP2* mRNA is subject to alternative splicing to generate *E1* and *E2* transcript isoforms that differ in the presence or absence of exon 2 (Kriaucionis and Bird, 2004). Importantly, these *MECP2* isoforms are alternatively polyadenylated (APA), producing four different 3' UTR lengths, including the unusually long 8.6-kb 3' UTR found in neurons (Singh et al., 2008). These distinct transcripts are potential platforms for differential post-transcriptional regulation.

RNA-binding proteins (RBPs) regulate diverse aspects of RNA biology, including stability and/or translation efficiency (Parker and Sheth, 2007). For example, Pumilio1 (PUM1) interacts with PUM1-binding elements (PBEs) in the 3′ UTR of target mRNAs, causing destabilization by recruiting deadenylase complexes (Goldstrohm et al., 2007; Van Etten et al., 2012). PUM1 also can facilitate miRNA-dependent silencing by inducing conformational changes in the 3′ UTR secondary structure of target genes to make miRNA seed sequences near PBE sites more accessible (Kedde et al., 2010; Miles et al., 2012). RBPs can control the translational efficiency of transcripts and their engagement with polysomes. This includes TIA1, which mediates translational silencing of transcripts containing adenine/uridine (AU)- or uridine (U)-rich sequence elements. Similar RNA targets are bound by the neuron-specific ELAVL-3/HuC protein. HuC is a member of a family of RBPs whose functions are intricately implicated in neuronal differentiation, maturation, and maintenance (Ince-Dunn et al., 2012; Simone and Keene, 2013).

Here we demonstrate that post-transcriptional regulatory mechanisms have a major role in determining MECP2 protein levels in the first steps of human neurodevelopment, as defined

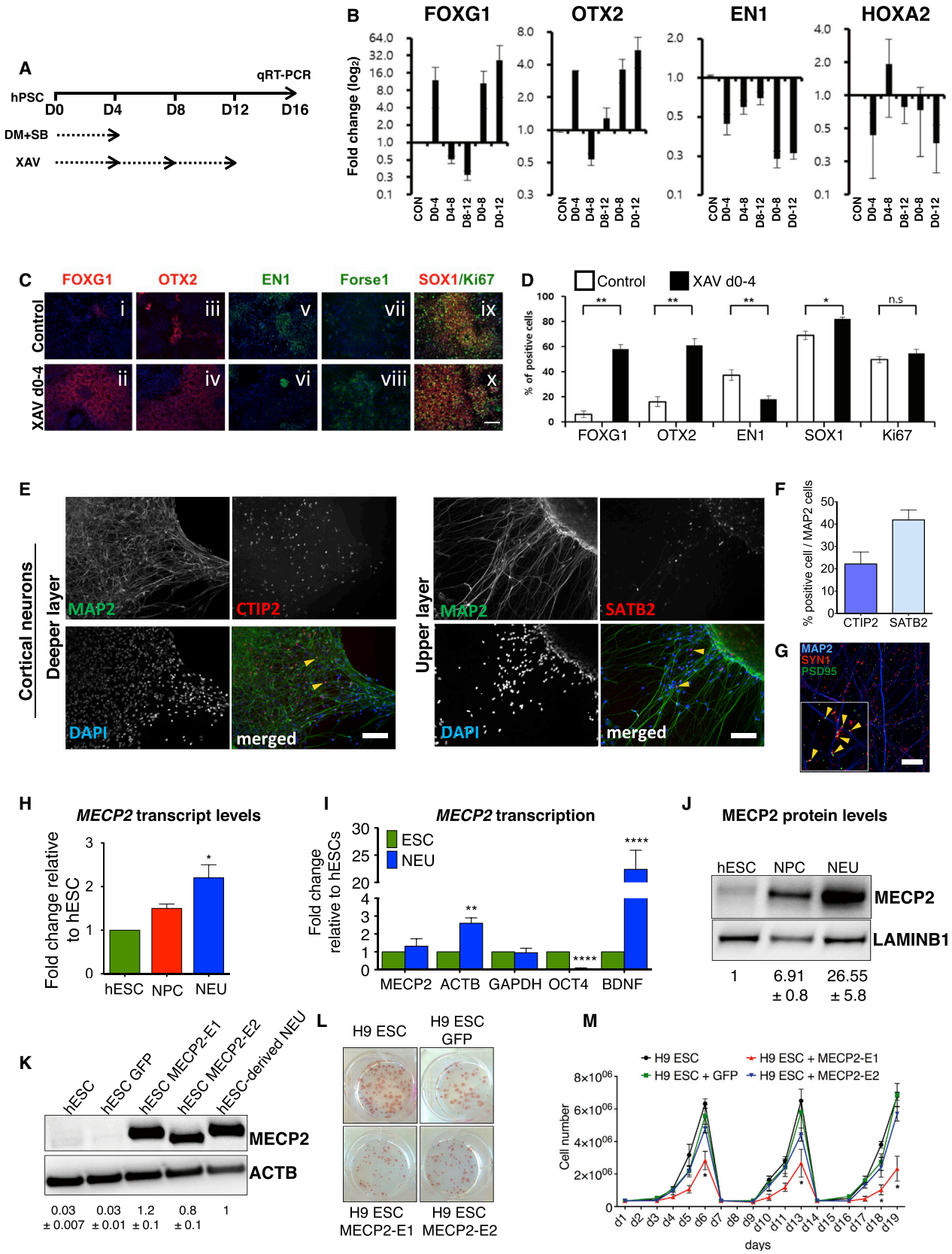

(legend on next page)

using a human embryonic stem cell (hESC) differentiation model that enriches for the generation of cortical neurons. As differentiation proceeds, *MECP2* transcripts with the long 3′ UTR (8.6 kb) are stabilized and MECP2 protein accumulates in neurons. We show that premature overexpression of high MECP2 protein levels in hESCs results in reduced stem cell proliferation. To safeguard against such a detrimental effect, the long isoform is actively transcribed in hESCs but is rapidly degraded, whereas the stable short isoform is translationally silenced. We characterize a sequence element present only in the long isoform that is recognized by PUM1, which acts together with the miRNAs hsa-miR-200a and hsa-miR-302c to destabilize the long *MECP2* transcript in hESCs. We also found that a U-rich sequence element present in the 3′ UTR of both isoforms is responsible for negative and positive translational regulation, where it is recognized by TIA1 in hESCs for translation repression and by HuC for translation enhancement in neurons. Our study shows how MECP2 protein levels are differentially regulated in hESCs and neurons, and it uncovers the combinatorial circuitry of multiple RBPs and miRNAs that regulate MEPC2 protein levels during neurodevelopment.

RESULTS

Recapitulation of Human Forebrain Development In Vitro

To investigate the post-transcriptional mechanisms of *MECP2* gene regulation during neurodevelopment, we established a protocol for the efficient generation of cortical neurons from human pluripotent stem cells. Cortical neurons arise in the dorsal/anterior domain of the developing brain (Hansen et al., 2011), and we hypothesized that this regional identity could be promoted by a dual-SMAD inhibition method coupled with inhibition of WNT signaling (Maroof et al., 2013; Nicoleau et al., 2013). The dual-SMAD inhibition resulted in a highly pure population of cells that stained for the neuronal progenitor markers SOX1, SOX2, NESTIN, and PAX6, but only a small fraction of cells expressed the anterior markers FOXG1 and OTX2 (Figures S1A–S1C). However, treatment of H9 hESCs with the WNT inhibitor XAV939 (XAV) over 12 days of neural induction remarkably enhanced the expression of anterior neural markers FOXG1 and OTX2, and it reduced the expression of midbrain and hindbrain markers EN1 and HOXA2 (Figures 1A, 1B, and S1D).

To determine the optimal temporal window of WNT inhibition for anterior specification of neural progenitor cells (NPCs), we dissected the 12 days into three stages of 4 days each and applied XAV as described in Figure 1A. The qRT-PCR revealed that treatment with XAV during the first 4 days showed effects comparable to the 12-day treatment (Figure 1B), in contrast with treatment over days 4–8 or days 8–12. Treatment with XAV during the first 4 days increased FOXG1$^+$ and OTX2$^+$ cells and decreased EN1$^+$ cells (Figures 1C [i–vi], 1D, S1E, and S1F). The Forse-1 marker of embryonic forebrain predominantly detected cells in the XAV-treated group (Figure 1C [vii and viii]). Interestingly, SOX1$^+$ cells increased with XAV treatment, suggesting that WNT inhibition can increase the efficiency of neural induction, possibly by suppressing commitment to the neural crest lineage (Menendez et al., 2011) (Figures 1C [ix and x] and 1D). Finally, we found no difference in Ki67$^+$ proliferating cells (Figures 1C [ix and x] and 1D). The robustness of this method was confirmed in a human induced pluripotent stem cell (iPSC) line previously generated in our lab (Cheung et al., 2011) (Figures S1E and S1F). In conclusion, our data demonstrate that WNT inhibition during the initial 4 days of dual-SMAD differentiation promotes the specification of NPCs with anterior fate.

To examine whether hESC-derived NPCs produced by this protocol generate cortical neurons, we further differentiated these cells using a previously reported neuronal differentiation method (Brennand et al., 2011). After 2 weeks, small clumps of PAX6$^+$ and cortical progenitor marker TBR2$^+$ cells were found (Figure S1G). Cells migrating out of the clumps were also Ki67$^-$ and DCX2$^+$ (Figure S1H), consistent with cortical progenitor molecular identity. After 9 weeks, MAP2$^+$ neuronal cells were co-labeled with markers for mature cortical neurons, including the cortical layer markers CTIP2 and SATB2 (Figures 1E and 1F). PSD95 and SYNAPSIN1 colocalized along MAP2$^+$ neuronal processes, indicating the formation of mature synaptic connections (Figure 1G). Collectively, our data suggest that dual-SMAD and WNT inhibition produces cortical progenitors that differentiate into mature cortical neurons.

MECP2 Is Post-transcriptionally Regulated during Human Neurodevelopment

We observed a significant discrepancy between the levels of *MECP2* transcript and protein over the course of neuronal

Figure 1. Fate Patterning of NPCs toward Anterior Neuronal Cells

(A) Schematic shows anterior neural cell differentiation by treatment with XAV over 12 days in three stages of 4 days each. Dorsomorphin + SB431542 (DM+SB).
(B) qRT-PCR shows increased expression of anterior markers (FOXG1 and OTX2) and decreasing expression of midbrain markers (EN1) and hindbrain (HOXA2) after XAV939 treatment of H9 hESCs (D0–4, D0–8, and D0–12).
(C and D) Immunofluorescence images and quantification of positive cells are shown. Scale bar, 100 μm.
(E) Immunofluorescence images after 9 weeks of neuronal differentiation (two bottom layers). Most cells were positive for the cortical neuron markers MAP2, CTIP2, or SATB2. Scale bars, 100 μm.
(F) Frequency of CTIP2$^+$ or SATB2$^+$ neurons is shown.
(G) Colocalization of PSD95 and Synapsin-1 along MAP2$^+$ neuronal processes is shown. Scale bar, 10 μm.
(H) qRT-PCR shows the small increase in *MECP2* mRNA steady state from hESCs to NPCs and neurons (n = 3).
(I) qRT-PCR of newly transcribed mRNAs from *MECP2* and controls *ACTB*, *GAPDH*, *OCT4*, and *BDNF* using the Click-It assay (n = 3) is shown.
(J) Western blot shows increased MECP2 protein levels in neurons compared to NPCs and hESCs (n = 3).
(K) Western blot shows hESC overexpressing the different *MEPC2* gene isoforms at levels comparable to hESC-derived neurons.
(L) Alkaline-phosphatase staining of hESC overexpressing *MEPC2* isoforms is shown.
(M) Proliferation assay with daily cell number counts. Cells were passed on days 1, 7, and 14 (*$p < 0.05$, **$p < 0.01$, and ****$p < 0.0001$; for Figure 1M *$p < 0.0001$; ANOVA, Bonferroni post-test). See also Figure S1.

differentiation. *MECP2* transcripts were detected in H9 hESCs and NPCs by qRT-PCR using a primer set designed to detect all *MECP2* transcript isoforms, and the steady-state levels increased by 2- to 3-fold in the hESC-derived neurons (Figure 1H). To investigate whether the modest increase in the total transcript levels is caused by increased transcription of *MECP2* in neurons, we measured the levels of *MECP2* nascent mRNAs (newly transcribed) in hESCs and neurons. Cells were pulse-labeled with 5-ethynyl uridine (EU) for 30 min and total RNA was extracted. Newly synthesized EU-RNAs were separated from the total RNA by biotinylation of EU using the click chemistry method (Jao and Salic, 2008), followed by pull-down of biotinylated EU-RNAs using streptavidin magnetic beads.

Using the captured RNA as a template for cDNA synthesis and qRT-PCR, we determined that there was no significant change in *MECP2* transcription efficiency between hESCs and neurons (Figure 1I). The controls indicated that *ACTB* may have been more actively transcribed in neurons but *GAPDH* transcription levels were equivalent between hESCs and neurons. As expected, *OCT4* was highly transcribed in hESCs while *BDNF* was highly transcribed in neurons. These results suggest that the increase in steady-state levels of *MECP2* transcripts is caused by differential mRNA stabilization in hESCs and neurons. Interestingly, despite the abundance of *MECP2* transcripts in hESCs and NPCs, we detected low levels of MECP2 protein levels by western blot in both cell types in contrast to the high levels present in neurons (Figure 1J). Taken together, these results show that *MECP2* is actively transcribed throughout human neurodevelopment, but protein levels are regulated by post-transcriptional mechanisms.

Premature MECP2 Overexpression in hESCs Affects Stem Cell Proliferation

To evaluate potential consequences of premature overexpression of *MECP2* in H9 hESCs, we overexpressed both *MECP2* gene isoforms (E1 and E2). We used lentiviral vectors lacking the *MECP2* UTRs, and we titrated infections to express the same physiological levels of MECP2 protein found in neurons (Figure 1K). Interestingly, we observed smaller Alkaline Phosphatase^{+} colony size of *MECP2*-overexpressing hESCs, suggestive of a deficit in cell proliferation (Figure 1L). To quantify the proliferation deficit, we counted the cell number over a period of 19 days and three cell passages. Figure 1M shows that hESCs overexpressing *MECP2-E1* had significantly reduced cell numbers of ~2-fold per passage compared to untransduced wild-type (WT) or GFP control cells. Together these data indicate that excess MECP2 protein is detrimental to hESCs. We therefore focused on defining mechanisms of *MECP2* post-transcriptional regulation in hESCs and neurons.

MECP2 Transcripts with the Long 3′ UTR Are Differentially Stabilized in hESCs and Neurons

To gain insight into the functional roles of the *MECP2* 3′ UTR in hESCs and neurons, we first characterized the levels of each of the four APA transcript variants (Figure 2A, arrowheads) during human neurodevelopment. To this end, we re-analyzed RNA sequencing (RNA-seq) data from the CORTECON database, which measured the changes in steady state of mRNAs at multiple points during the course of neuronal differentiation from hESCs (van de Leemput et al., 2014). We observed robust levels of the short (0.1 kb) and the long (8.6 kb) isoforms of *MECP2* mRNAs in hESCs and neurons, in contrast to negligible amounts of the other two intermediate isoforms (Figure 2B). While the short isoform levels were consistently maintained during neurodevelopment, the steady-state levels of the long isoform progressively increased (Figure 2B). We validated the CORTECON data by qRT-PCR using our hESC, NPC, and neuron RNA samples by measuring the levels of total and long 3′ UTR *MECP2* transcripts, using primer sets against exons 3 and 4 (present in all isoforms, Figure 2A, red line) and a region immediately upstream of the 8.6-kb polyadenylation (PA) site, respectively (Figure 2A, blue line). In agreement with the CORTECON dataset, the qRT-PCR showed an increase in the total levels of *MECP2* transcripts of ~3-fold, while the steady-state level of the long isoform increased ~8-fold in neurons (Figure 2C), raising the possibility that the stability of the long isoform may be post-transcriptionally regulated (Figure S2).

To determine the relative stability of *MECP2* transcripts in hESCs and neurons, we measured the half-life of the total and long *MECP2* transcripts. In hESCs the half-life of total *MECP2* was ~3 hr, whereas the long *MECP2* transcript isoform was relatively unstable with a half-life of less than 1 hr (Figure 2D). In contrast, in neurons the degradation of the long isoform was barely detectable even after 5 hr, suggesting a dramatic stabilization of the transcript. As expected, the unstable *MYC* transcript used as a control had a short half-life of less than 1 hr in both cell types. Together with the transcription efficiency assay (Figure 1I), these data suggest that both long and short *MECP2* transcripts are produced in hESCs, but the long transcript is rapidly degraded and therefore accumulates to lower steady-state levels than the short isoform. As neuronal differentiation progresses, the long isoform becomes dramatically more stable and accumulates in neurons to levels equivalent to the short isoform.

The 3′ UTR Directs Post-transcriptional Regulation of *MECP2* in hESCs and Neurons

Since *MECP2* transcripts contain an unusually long 3′ UTR that is retained preferentially in neurons, we reasoned that it may contain sequence elements with important regulatory functions. To identify functionally significant regions, we cloned fragments of the *MECP2* 3′ UTR in luciferase reporter plasmids for transfection into hESCs and neurons, and we measured mRNA levels and luciferase activity (Figure 3A). The minimal regions with the largest differences between hESCs and neurons were the fragments corresponding to nucleotides 4,265–5,677 and 1–149 of the 8.6-kb 3′ UTR. In comparison to the control plasmid (pLUC-*GAPDH*), reporter pLUC-4,265–5,677 had reduced reporter mRNA, suggesting that it contains sequence elements capable of mRNA destabilization and, consequently, lower luciferase activity in hESCs. Importantly, reporter pLUC-1–149 luciferase activity was reduced in hESCs and enhanced in neurons, but the reporter mRNA levels were unchanged, suggesting that this fragment contains sequence elements capable of regulating translation.

Given the high sequence conservation throughout the 3′ UTR among other species, it is not surprising that all fragments

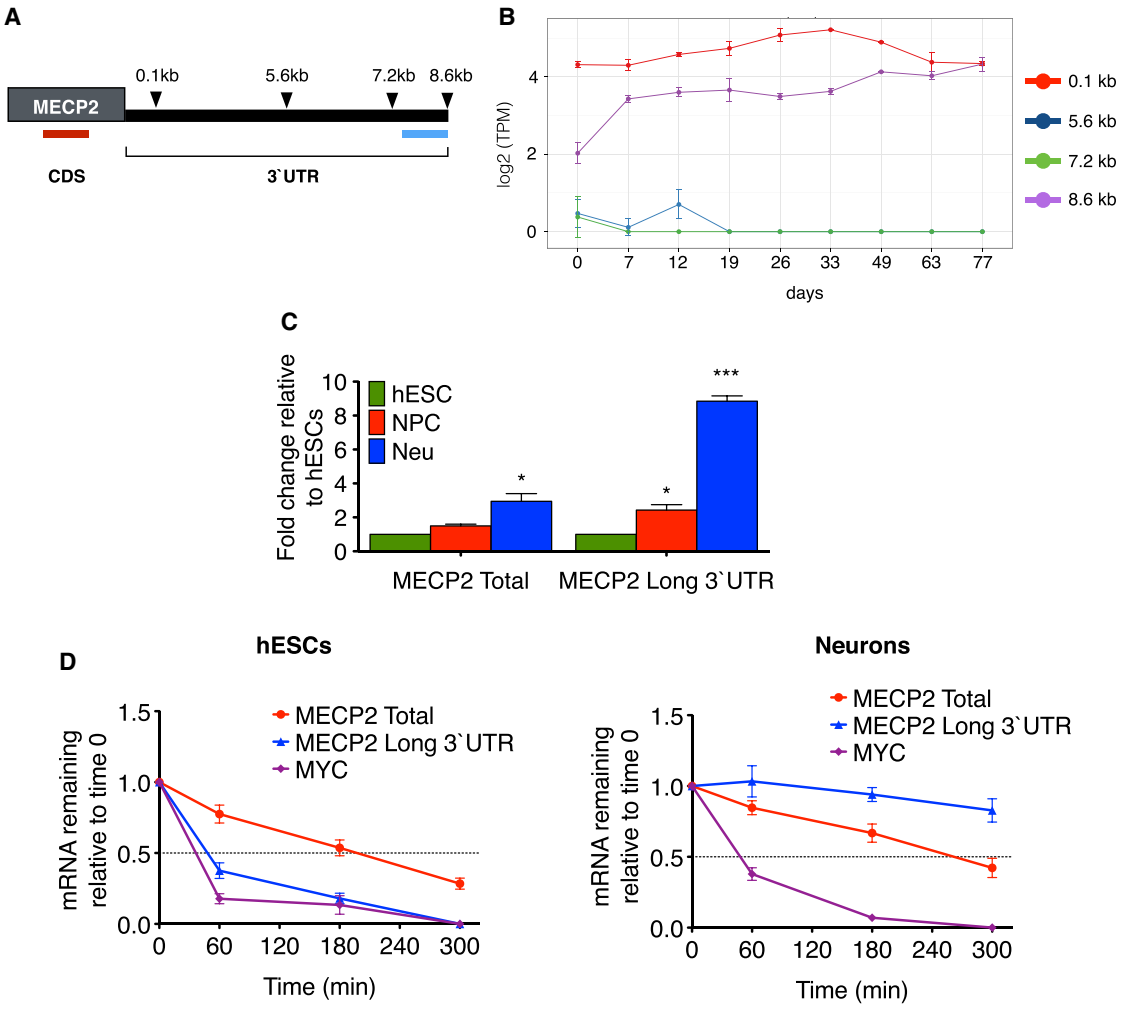

Figure 2. *MECP2* Transcripts Are Differentially Stabilized during Neurodevelopment

(A) Schematic representation of the long 3′ UTR of *MECP2* mRNA. Arrowheads indicate PA sites. Red and blue lines indicate regions targeted for qRT-PCR of the total or long *MECP2* transcripts, respectively.

(B) Quantification of the four APA isoforms of *MECP2* mRNA produced during neurodevelopment using RNA-seq data from the CORTECON Database is shown.

(C) qRT-PCR confirms changes in *MECP2* transcript levels (total and long) during neurodevelopment (n = 3).

(D) Effect of neuronal differentiation on the half-life of *MECP2* transcripts determined by qRT-PCR (n = 3). Quantification of *MYC* was used as a control. Error bars, SEM; *p < 0.05 and ***p < 0.001 (ANOVA, Bonferroni post-test). See also Figure S2.

had some reduction in luciferase reporter activity in hESCs. This includes the pLUC-1–4,508 fragment that contains the known miRNA site functioning in fetal brain (Han et al., 2013), which had a modest effect on post-transcriptional regulation in our experimental system. Taken together, these results show that the *MECP2* 3′ UTR contains previously uncharacterized sequence elements capable of regulating mRNA stabilization and translation in hESCs and neurons, with the most differentially active regions being located in fragments 4,265–5,677 and 1–149.

Identification of Candidate AU-Rich Sequences and RBPs

Stretches of AU-rich sequences are known to be targeted by RBPs and regulate mRNA stability and translation in cells including hESCs (Yokoshi et al., 2014). Sequence examination identified long, highly conserved, AU-rich sequences in regions located between 4,265–5,677 and 1–149. To directly evaluate the interaction of these two conserved regions with RBPs in hESCs, we performed RNA electrophoretic mobility shift assays (REMSAs). Shifted bands were produced in the presence of hESC protein extract and competed by excess specific unlabeled fragments, but not non-specific tRNA and reverse-strand competitor fragments (Figure 3B). These results demonstrate that the two candidate regions interact with RBPs present in hESCs.

Affinity purification mass spectrometry assay was performed to identify RBPs from hESCs and neurons that interact with the *MECP2* 3′ UTR fragments. A number of proteins were associated with the two fragments (Table S1). However, the majority of these

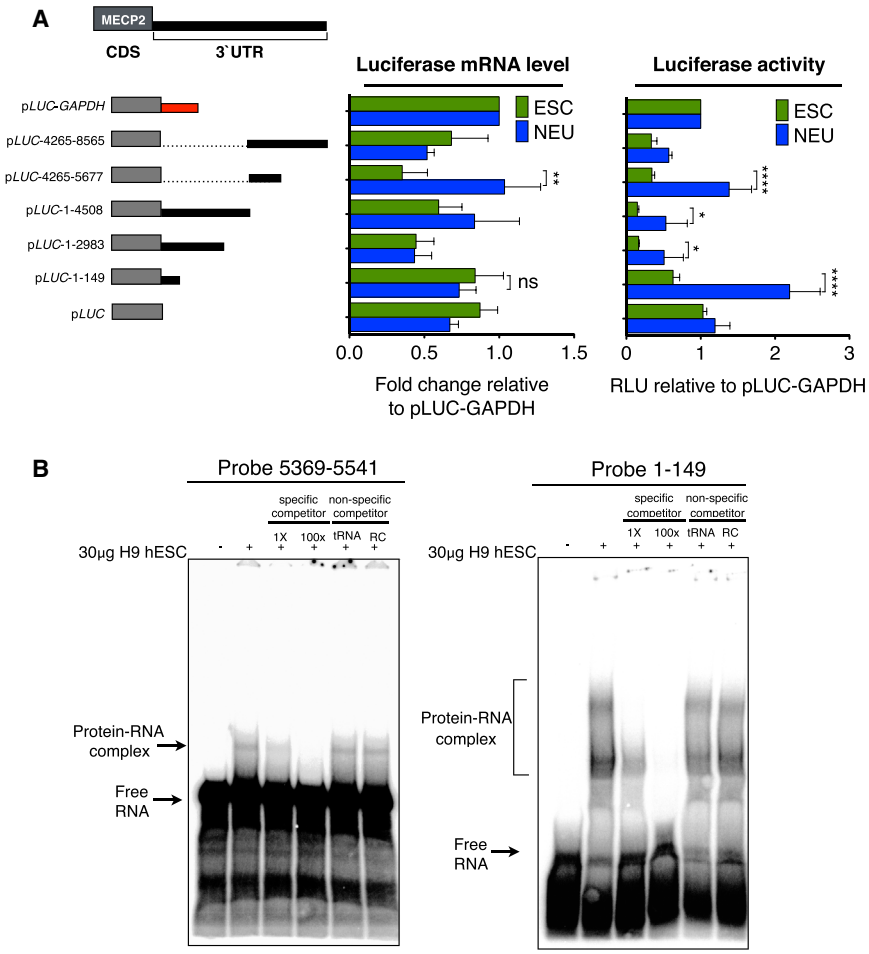

Figure 3. The 3′ UTR of *MECP2* Contains Sequence Elements Capable of Post-transcriptional Regulation

(A) Schematic representation of reporter plasmids used for luciferase assays. Numbers represent the nucleotide position at the beginning and end of each 3′ UTR fragment. Luciferase activity and mRNA levels are plotted relative to control pLUC-*GAPDH* (n = 10–24). RLU, relative light units. Error bars, SEM; *p < 0.05, **p < 0.01, and ****p < 0.001; ns, not significant (ANOVA, Bonferroni post-test).

(B) REMSA using RNA probes in the presence of hESC protein extracts. See also Figure S3.

RBP candidates have redundant consensus-binding sites that are widely distributed throughout the *MECP2* 3′ UTR (Figure S3), and therefore, they would be expected to have widespread effects on multiple regions. We narrowed the search for candidate RBPs to those with consensus sequences in the most important regions determined by reporter assays. In fragment 5,369–5,541, PUM1 was the only RBP candidate with potentially high binding specificity known to participate in mRNA destabilization. In fragment 1–149, the only RBPs with known functions related to translational regulation that shared the same consensus-binding site were TIA1 and HuC (ELAVL3).

PUM1 Destabilizes the Long Isoform of *MECP2* Transcripts in hESCs and NPCs via a Conserved PBE

Further investigation of the *MECP2* 3′ UTR sequence revealed two putative PBEs (5′-UGUANAUA/U-3′) (Van Etten et al., 2012) at positions 1,103–1,110 (PBE1) and 5,489–5,496 (PBE2). The latter site was located in the probe used for both the RNA gel shift and affinity purification assays (Figure 4A). Sequence alignment (Figure S4A) showed that PBE1 was moderately conserved, while PBE2 was highly conserved and present in all species analyzed. To rapidly test whether these elements confer differential post-transcriptional regulation via PUM1 interaction, we co-transfected the luciferase reporter vectors with plasmids for *PUM1* or *GFP* overexpression in 293T cells. *PUM1* overexpression significantly reduced luciferase activity of the two reporters containing PBE2, but not PBE1 (Figure 4B). In contrast, knockdown of *PUM1* using two independent small interfering RNAs (siRNAs) increased reporter activity of the two PBE2-containing plasmids (Figure S4B). Moreover, the half-life of the pLUC-4,265–5,677 reporter mRNA (containing PBE2) in 293T was reduced to 3 hr by *PUM1* overexpression compared to >6 hr in the GFP control. The half-life was reciprocally increased by knockdown of *PUM1* by both siRNAs in comparison to the control knockdown (Figure 4C). In contrast, PUM2 had no effect in the reporter studies (Figure S4C). These results demonstrate that PUM1 acts in *trans* to destabilize reporter transcripts containing the conserved PBE from the 3′ UTR of *MECP2*.

We next confirmed the importance of the active sequences in PBE2 by site-directed mutagenesis. We generated two mutant reporters containing either a deletion of PBE2 (PBE del) or a change of the first half of the sequence element (PBE mt) (Figure 4D). Indeed, both deletion and mutation of PBE2 abolished the inhibitory effects of *PUM1* overexpression in 293T cells and reversed the increase in reporter activity observed after *PUM1* knockdown (Figure 4D). Importantly, we found that deletion or mutation of PBE2 also significantly increased reporter activity in hESCs (Figure 4E). Notably, reporter activity did not completely recover to control levels, suggesting that additional functional sequences outside PBE2 also are recognized in hESCs.

Because *MECP2* transcripts are also post-transcriptionally regulated in NPCs, we studied the effects of *PUM1* knockdown in these cells. Indeed, reduction of *PUM1* levels by both small hairpin RNAs (shRNAs) induced accumulation of the total fraction of *MECP2* transcript (Figure S4D). Western blot analyses showed that PUM1, but not the ACTB control, was reduced in the knockdowns and that MECP2 protein levels were slightly

increased in NPCs, as expected (Figure S4E). Accordingly, knockdown of *PUM1* in neurons induced endogenous MECP2 protein (Figure 4F), whereas *PUM1* overexpression reduced MECP2 protein levels (Figure 4G). Multiple attempts at PUM1 knockdown for 5 days with shRNAs or siRNAs in hESCs were compromised by cell morphology and proliferation changes (data not shown). Taken together with the reporter studies, these results show that PUM1 controls endogenous MECP2, consistent with its ability to destabilize the long mRNA isoform.

PUM1 Interacts and Colocalizes with *MECP2* in hESCs

To test the association of PUM1 with endogenous *MECP2* mRNA in hESCs, we performed RNA immunoprecipitation (RIP) assays using PUM1 antibody. RIP followed by qRT-PCR revealed that both total and long isoform *MECP2* transcripts were bound by PUM1 protein in hESC extracts (Figure 5A). The known PUM1 targets *E2F3* and *p27* also were associated with PUM1 in our conditions. In contrast, neither *18S* rRNA nor *GAPDH* mRNA was detected with PUM1 antibody, indicating the specificity of PUM1/RNA interactions.

We confirmed colocalization in hESCs of endogenous *MECP2* transcripts with PUM1 protein by ImmunoRNA- fluorescence in situ hybridization (FISH) (Figures 5B–5G). One RNA probe set detected total *MECP2* transcripts by RNA-FISH and a second set detected the long isoform. As expected, significantly more puncta corresponding to the total fraction (Figure 5B, red puncta) were observed than puncta specific for the long isoform only (Figure 5B, green puncta). Many RBPs, including PUM1, can promote the assembly of target mRNAs into RNA granules (Parker and Sheth, 2007; Van Etten et al., 2012). The immunoRNA-FISH signals showed PUM1 in green foci that were predominantly outside the nuclei, and the total fraction of *MECP2* transcripts (short and long isoforms) was present in defined red focal structures (Figure 5C). A proportion of *MECP2* transcript puncta colocalized with PUM1 in all three dimensions, as measured in the acquired confocal z stacks (Figures 5C and 5D). Interestingly, probes that detect only the long isoform had significantly increased puncta colocalization with PUM1 foci (Figures 5D and 5E). PUM1 knockdown for 2 days using two independent siRNAs demonstrated the specificity of the antibody (Figure 5F), and a non-specific control RNA hybridization did not produce puncta (Figure 5G). These results confirm that the long *MECP2* isoform preferentially colocalizes with PUM1, consistent with the presence of the PBE2 site only in this isoform. Overall, PUM1 colocalization with *MECP2* mRNA is compatible with an in vivo interaction with the long *MECP2* isoform in hESCs, and it agrees with the RIP assay findings.

MECP2-null iPSC-derived neurons display altered morphology consisting of reduced dendritic length, arborization complexity, and soma size (Cheung et al., 2011; Li et al., 2013). To test whether the decrease in MECP2 protein levels in neurons elicited by PUM1 overexpression would recapitulate the typical abnormal phenotype, we performed morphological measurements on these neurons. To that end, we overexpressed *PUM1* (or *GFP* as the negative control) in neurons and measured dendrite complexity, length, and soma size (Figure S5A). As expected, *PUM1* overexpression in neurons induced similar morphological changes as those observed in *MECP2*-null iPSC-derived neurons, with impaired dendritic branching as measured by Sholl analysis, shorter dendrites, and smaller soma sizes (Figures S5B–S5F).

miR-200a and 302c Destabilize *MECP2* Independently of PUM1 in hESCs

Having firmly established that PUM1 regulates *MECP2* expression, we next sought to explore the underlying mechanisms. PUM1 can facilitate access of miRNAs to their seed sequences by alleviating high-energy secondary structures in the 3′ UTR of target mRNAs (Kedde et al., 2010; Miles et al., 2012). In silico secondary structure prediction suggested that very stable secondary structures surround PBE2 (Figure S6A). To investigate whether PUM1 acts in cooperation with miRNAs to reduce abundance of the long *MECP2* transcript in hESCs, we used TargetScan (http://www.targetscan.org) to predict potential miRNA-binding sites surrounding PBE2. hsa-miR-200a and hsa-miR-302c were selected as candidates for further analysis, since they are highly expressed in hESCs and repressed upon differentiation (Judson et al., 2009; Peng et al., 2012). As noted above, the luciferase reporter fragments containing the deletion or mutation of the PBE2 element did not completely reverse the luciferase activity in hESCs back to basal levels (pLUC-*GAPDH*), indicating that other repressing elements were present near PBE2.

To investigate the possible contribution of miR-200a and miR-302c in *MECP2* repression, we co-transfected mimic-miRNA molecules corresponding to the endogenous miRNAs together with the luciferase reporter vector containing PBE2 and the predicted miRNA-binding sites. Both mimic-miRNAs independently reduced reporter activity in 293T cells, and the reduction was lost using a mimic-miRNA control that had no complementarity with any human miRNA and after site-directed mutagenesis of the seed sequences of each miRNA (Figure 6A).

To evaluate whether PUM1 facilitates miR-dependent repression of *MECP2*, we co-transfected the mimic-miRNAs with the luciferase reporters containing the mutation or deletion of PBE2. Reduced reporter activity elicited by each miRNA was more pronounced when the PBE was intact, but reporter activity generally persisted without a functional PBE (Figure 6B, black bars). This result suggests that PUM1 binding at PBE2 has minimal impact on miRNA function. To further test whether PUM1 cooperates with the miRNAs to reduce reporter activity, we overexpressed PUM1 and the miRNAs in 293T cells. Indeed, PUM1 overexpression alone reduced reporter activity to ~0.5 relative light units (RLU), which was reverted back to ~1.0 as expected in PBE2 mutants (Figure 6B, orange bars). The role of the miRNAs was shown by the further reduction in reporter activity to ~0.3 RLU by co-transfection of the mimic-miRNAs. Moreover, the mimic-miRNAs could still repress the reporter activity to ~0.5 RLU even when the overexpressed PUM1 could not bind to the PBE2 in the deletion or mutant reporters. These results indicate that the miRNAs and PUM1 act independently but have a combinatorial repressive effect on the long isoform of *MECP2* mRNA.

To complement this analysis, we investigated the effect of the miRNAs on endogenous *MECP2* in hESCs using two independent approaches. First, we inhibited each of the miRNAs in

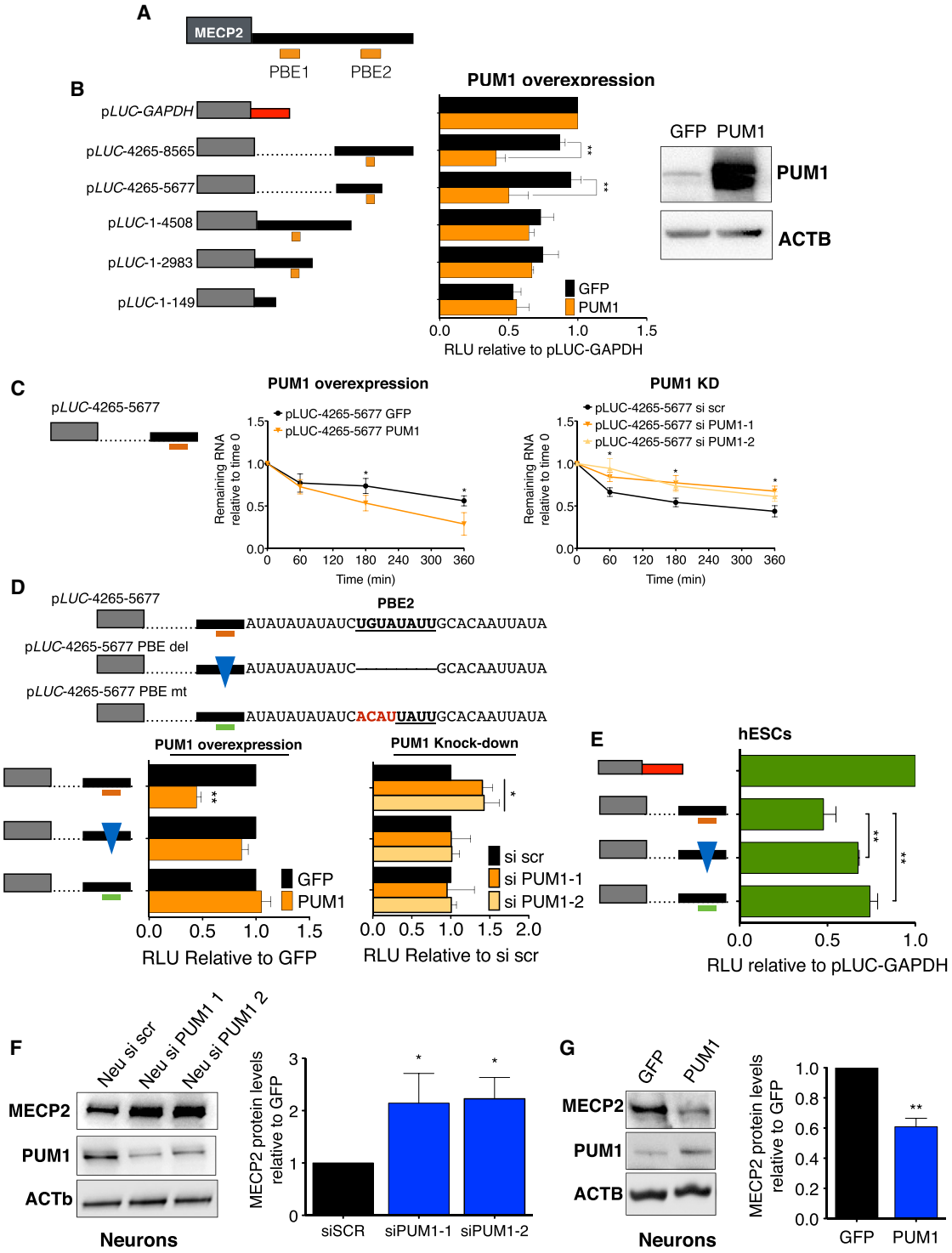

Figure 4. PUM1 Destabilizes *MECP2* Transcripts

(A) Schematic representation shows the two PBEs present in the 3′ UTR of *MECP2*.

(B) Luciferase assay in 293T cells. The inset displays changes in PUM1 protein levels after overexpression (n = 10–16).

(C) qRT-PCR shows the effect of PUM1 overexpression or knockdown on the half-life of the reporter plasmid containing PBE2 (n = 3).

(D) Top: Schematic representation shows PBE2 and deletion (blue triangle) or mutation (green line) clones generated by site-directed mutagenesis. Bottom: Luciferase assay of reporter vectors containing WT or mutant versions of PBE2 after PUM1 overexpression or knockdown is shown. Data are plotted relative to GFP or siRNA scrambled (scr) controls for each reporter condition (n = 3).

(legend continued on next page)

hESCs by transfection of anti-miRNAs with reverse complementarity to the endogenous miRNAs to bind and inhibit their activity. In agreement with the luciferase reporter experiments, we observed a significant increase in the steady-state levels of the long isoform after inhibition of each miRNA (Figure 6C), although no change was observed in the total fraction. Interestingly, the increase in the levels of the long isoform was accompanied by a significant increase in the levels of the *MECP2-E1* transcript isoform, but not *MECP2-E2.* In addition, we transfected hESCs with target protector RNAs for both miRNA sites. These are long synthetic RNAs with reverse complementarity to the specific miRNA seed sites and surrounding sequence in the *MECP2* transcript. They impair the ability of the endogenous miRNAs to bind *MECP2* transcripts, and, due to their length, they are not substrates for RISC-dependent miRNA-guided RNA degradation. Similar to the anti-miRNAs, both target protector RNAs independently increased levels of the long *MECP2* isoform, and the miRNA-200a protector increased levels of the *MECP2-E1* isoform (Figure 6D). These data suggest that the *MECP2-E1* isoform is composed of transcripts containing the long 3′ UTR. Taken together, these results confirm that *MECP2* mRNA levels are reduced in hESCs by a combinatorial effect of PUM1 and miR-200a and miR-302c.

Translational Regulation of *MECP2* Is Mediated by a U-Rich Element in the 3′ UTR

The post-transcriptional regulation of *MECP2* in cells also is controlled at the translational level. To evaluate translational regulation of endogenous *MECP2* transcripts, we performed polysome-profiling assays in hESCs and neurons, and we quantified the total fraction of *MECP2* mRNA in the different polysome fractions (Figure S7A). The majority of *MECP2* transcripts were present in the free-monosome fraction in hESCs, whereas in neurons most *MECP2* transcripts were detected in the heavy-polysome fractions (Figure 7A). These results confirm that endogenous *MECP2* transcripts are translationally silenced in hESCs, given that they are not engaged in active translation. As differentiation progressed, two effects were observed: the long transcript isoform accumulated to greater levels and the corresponding association of *MECP2* transcripts with polysomes increased, resulting in MECP2 protein synthesis and accumulation in neurons.

Sequence inspection revealed a conserved U-rich sequence at 102–127 immediately upstream of the first PA site of *MECP2* 3′ UTR (Figure S7B). To evaluate its role, we mutated every second T into a C (Figures 7B and S7B). Indeed, this mutation (pLUC-1–149_T > C) completely abolished the reduction in translation seen for the WT sequence in hESCs as well as the enhancement of translation in neurons when compared to basal levels in the control pLUC-*GAPDH* (Figure 7B), whereas there was no change in reporter mRNA levels. These results demonstrate that the U-rich element was required for translational regulation of the luciferase reporter in both hESCs and neurons. Given that MECP2 protein is poorly detected in hESCs, we infer that the element prevents translation of both the small and large transcript isoforms in hESCs. In neurons, translation is enhanced by the same element and should function on both isoforms, unless the short isoform is a completely abortive transcript that fails to be translated in neurons.

Translation of *MECP2* Transcripts Is Regulated by the RBPs TIA1 and HuC

The fact that the same U-rich element induces opposite outcomes for reporter protein levels in hESCs and neurons suggests that cell-type-specific factors regulate the translation of MECP2. Two proteins identified in our affinity purification experiments were the translational regulators TIA1 and HuC. To assess whether translational repression of *MECP2* transcripts is mediated by TIA1, we first tested the luciferase activity of our reporter constructs after *TIA1* knockdown in hESCs (Figure 7C). Interestingly, the luciferase activity of the construct containing the WT 1–149 region was increased to that of basal levels after *TIA1* knockdown using two independent siRNAs in the hESCs, whereas no changes were observed in the T > C mutant reporter in hESCs (Figure 7C) or 293T cells (Figure S7C). Importantly, we confirmed that endogenous MECP2 protein levels were significantly increased in hESCs after the reduction of TIA1 by the siRNAs (Figures 7D and S7D). Additionally, we demonstrated that TIA1 protein levels were significantly lower in neurons compared to hESCs, which could in part explain a lower effect of TIA1-mediated translation repression of *MECP2* in neurons (Figure S7E). We also demonstrated that TIA1 interacted with *MECP2* transcripts. ImmunoRNA-FISH showed that TIA1 granules partially colocalized with both *MECP2* transcript isoforms at similar frequencies (Figures 7E and 7F). Knockdown of TIA1 with two independent siRNAs demonstrated the specificity of the antibody (Figure 7G). In addition, RIP followed by qRT-PCR showed that both total and long *MECP2* transcripts associated with TIA1 protein in hESCs and that the association was less prominent in neurons (Figure S7F).

To investigate the roles of HuC protein in translation enhancement of MECP2 protein in neurons, we repeated the luciferase reporter assays after knockdown of *HuC*. Indeed, the increased reporter activity induced by the 1–149 fragment was lost after HuC repression by siRNAs in neurons (Figure 7H). Interestingly, overexpression of *HuC*, but not *HuD*, induced the reporter activity of pLUC-1–149 in 293T cells (Figure S7G). Moreover, we confirmed the positive regulation of endogenous neuronal MECP2 protein levels after *HuC* overexpression (Figures 7I, 7J, and S7H). Finally, we demonstrated the association between HuC protein and *MECP2* transcripts by RIP qRT-PCR in neuron extracts (Figure S7I). Taken together, these results demonstrate that in hESCs *MECP2* transcripts are directly bound and translationally repressed by TIA1. Upon differentiation to neurons, TIA1

(E) Luciferase assay in hESCs using reporter plasmids containing WT or mutant PBE2 (n = 3) is shown.
(F and G) Western blot shows increase or decrease of MECP2 protein levels after knockdown or overexpression of PUM1 in neurons, respectively (n = 3). Error bars, SEM; *p < 0.05, **p < 0.01, and ****p < 0.001 (ANOVA, Bonferroni post-test for luciferase assay and qRT-PCRs, or SEM for western blots by Student's t test). See also Figure S4.

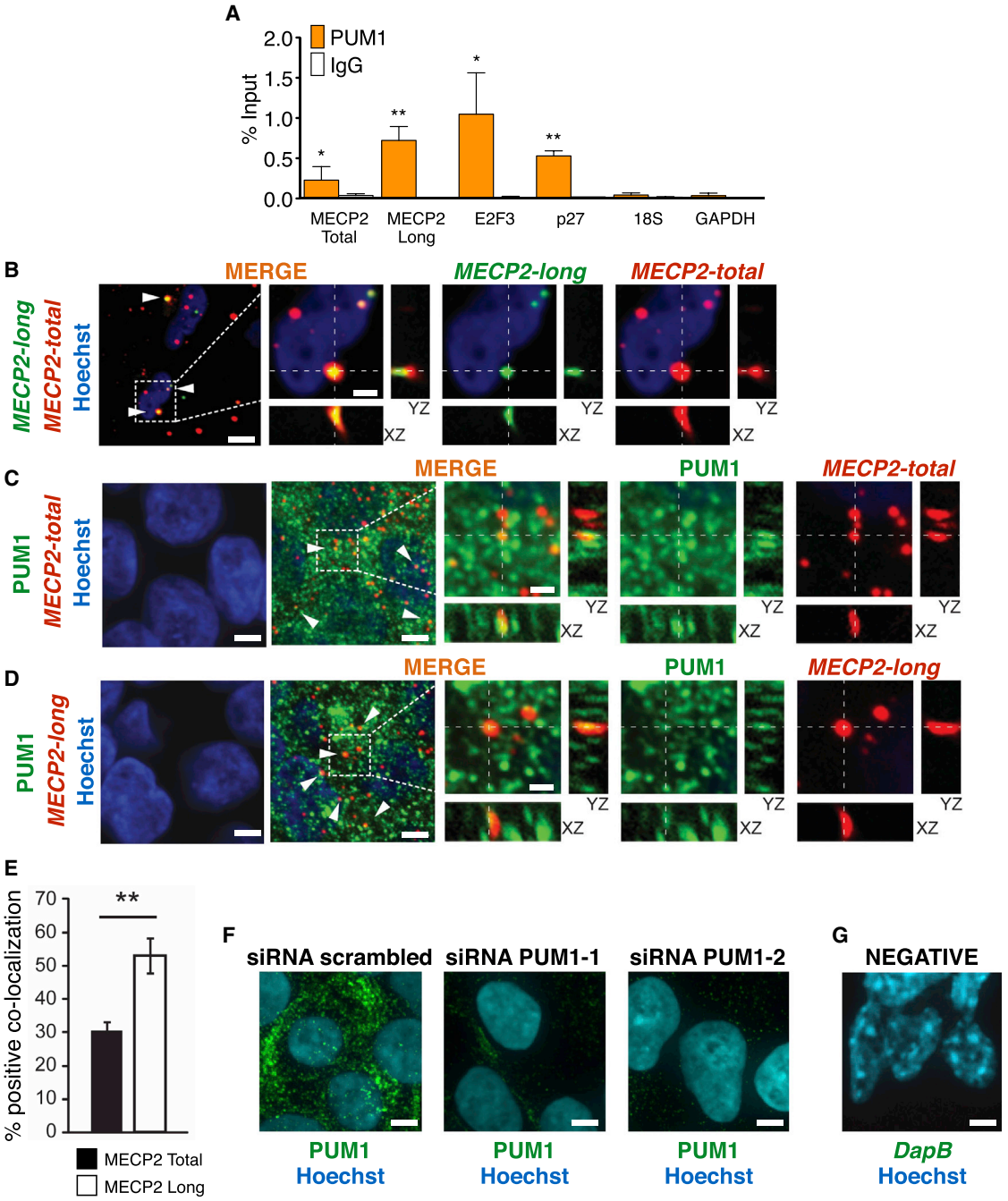

Figure 5. PUM1 Directly Associates with *MECP2* Transcripts

(A) RIP-qRT-PCR using PUM1 antibody and isotype IgG control in hESCs extracts shows the association between PUM1 and *MECP2* transcripts (n = 3). Error bars, SEM; *p < 0.05 and **p < 0.01 (ANOVA, Bonferroni post-test).

(B–D) Confocal imaging of RNA-FISH using probes against *MECP2* total (C) or long transcripts (D) and PUM1 immunostaining, counterstained with Hoechst33258. Boxed areas show higher magnification. Arrowheads, colocalization puncta.

(E) Quantification of PUM1/*MECP2* colocalization is shown. Scale bars, 10 μm (B, low magnification), 2.5 μm (B–D, high magnification), 5 μm (C, D, F, and G, low magnification). Error bars, SEM; n = 60 cells each; **p < 0.01 (Student's t test).

(F) PUM1 antibody specificity is demonstrated by confocal imaging of immunostained hESC after knockdowns.

(G) Negative control for RNA-FISH using a non-specific *DapB* probe is shown.

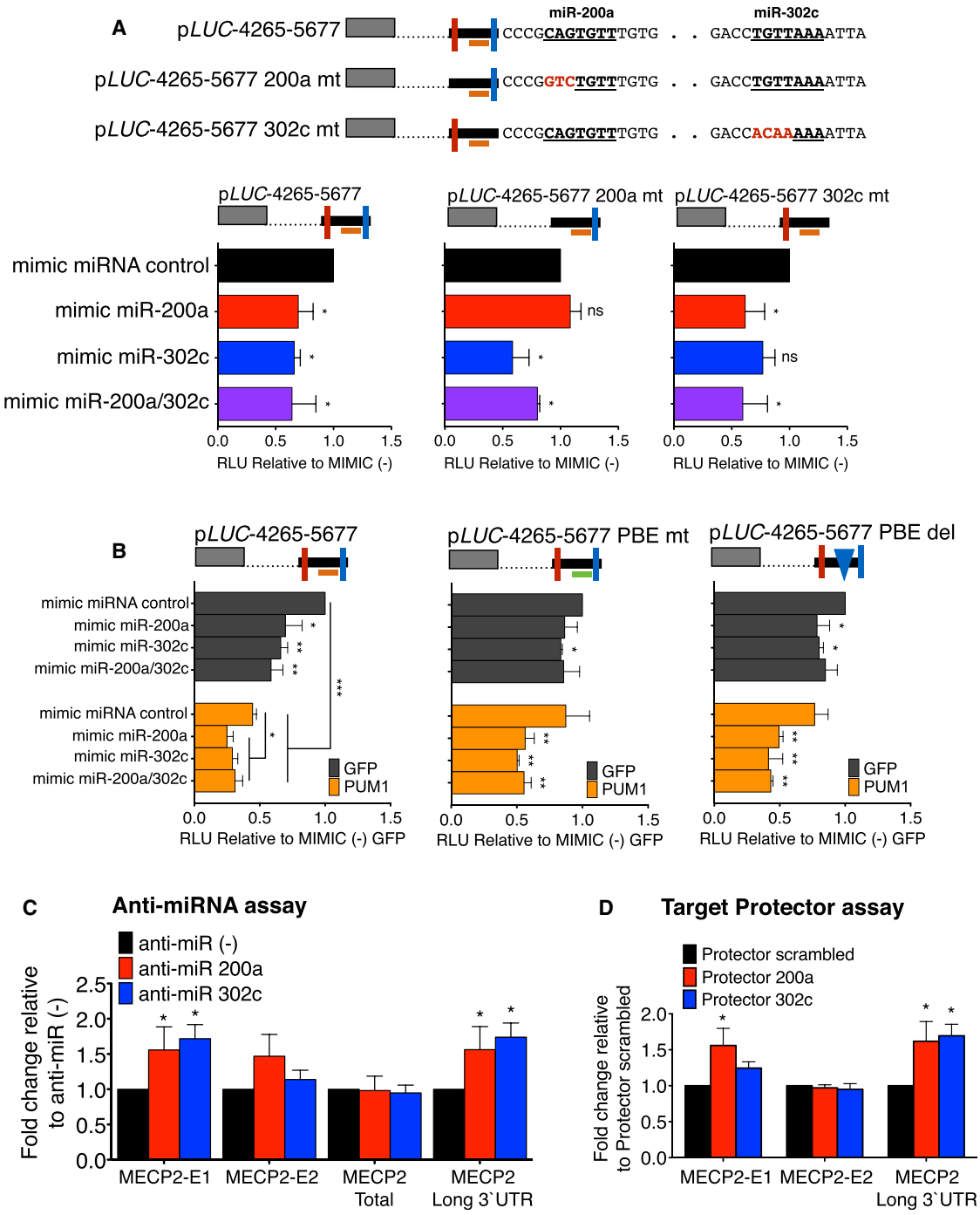

Figure 6. miRNAs 200a and 302c Destabilize *MECP2* Long Transcripts Independent of PUM1

(A) Schematic representation of luciferase reporter plasmids harboring the WT (*pLUC*-4,265–5,677) or mutant binding sites for miRNAs 200a (*pLUC*-4,265–5,677 200a mt) and 302c (*pLUC*-4,265–5,677 302c mt) (top). Red and blue lines represent the presence of the WT binding sites for miRNAs 200a or 302c, respectively, and orange line represents PBE2. Luciferase assay in 293T cells using the plasmids shown above and overexpression of each mimic-miRNA (bottom) are shown. Results are plotted relative to mimic-miRNA control (negative control, n = 3).

(B) Luciferase assay in 293T cells using the plasmid harboring the PBE2 WT (left), PBE2 mut (middle), or PBE2 del (right) and overexpression of each mimic-miRNA and PUM1 (n = 3) are shown.

(C) qRT-PCR in hESCs after repression of each miRNA using anti-miRs (n = 3) is shown.

(D) qRT-PCR in hESCs after transfection of target protector synthetic RNAs specific for the *MECP2* transcript seed sites for miRNAs-200a and -302c. Error bars, SEM; *p < 0.05, **p < 0.01, ***p < 0.005, and ****p < 0.001 (ANOVA, Bonferroni post-test). See also Figure S6.

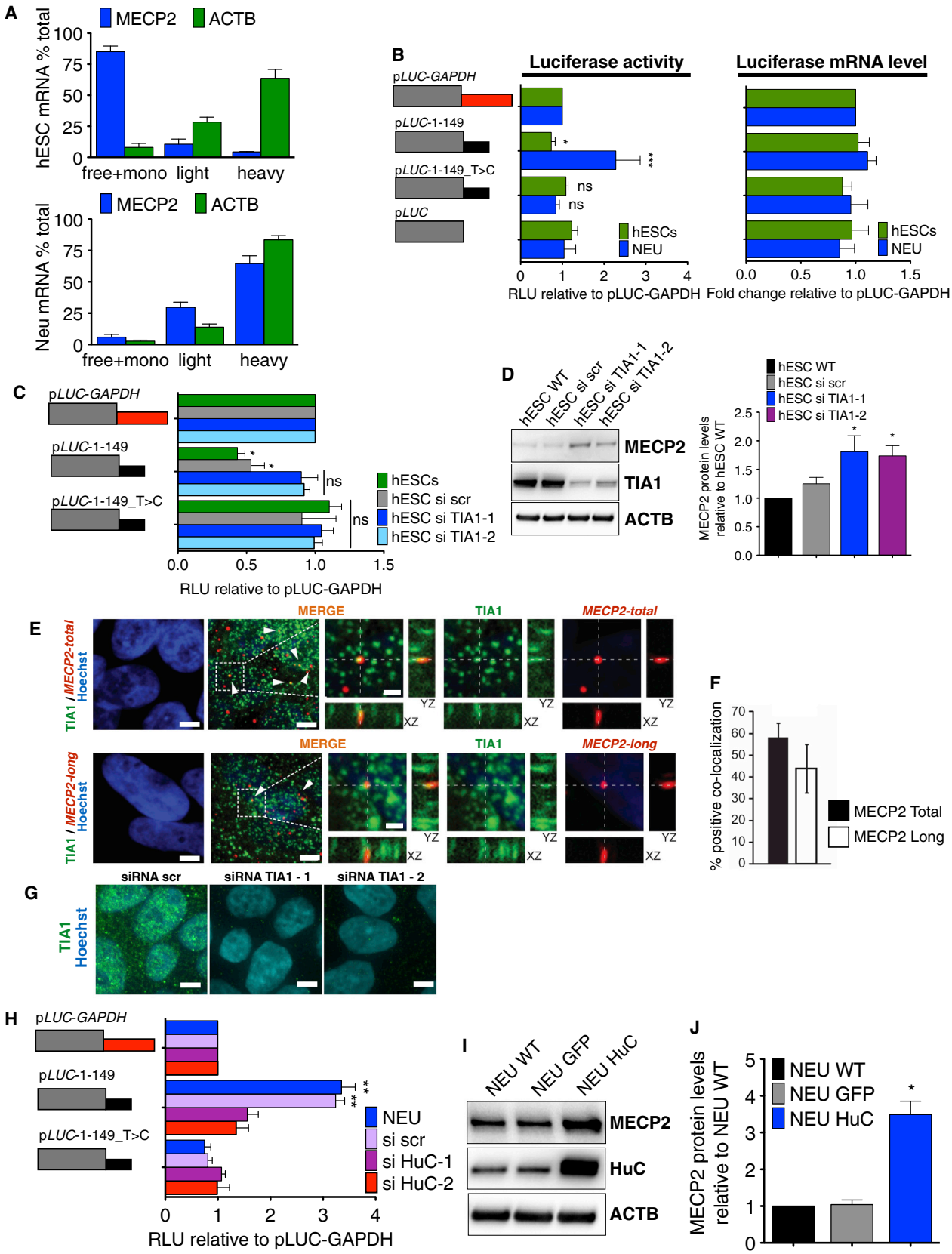

(legend on next page)

levels and its association with *MECP2* transcripts are reduced, while HuC contemporaneously increases, which together lead to a substantial increase in the translation of *MEPC2*.

DISCUSSION

In the present study, we identified key post-transcriptional regulators of MECP2 protein levels during human neurodevelopment. Our data revealed that RBPs and miRNAs interact with sequences in the conserved 3′ UTR of *MECP2* transcript to control mRNA stability and translational efficiency. First, the long 3′ UTR isoform of *MECP2* mRNA is destabilized in hESCs via the concerted action of PUM1 and two pluripotency-associated miRNAs. Second, the translational efficiency of all *MECP2* transcripts is repressed in hESCs via interactions of the 3′ UTR with TIA1. Together these pathways reduce the half-life of *MECP2* transcripts and minimize ribosome engagement, thereby preventing MECP2 protein accumulation in hESCs. We demonstrated that overexpression of *MECP2 E1* protein in the absence of the 3′ UTR in hESCs affects stem cell proliferation. Upon differentiation into neurons, a switch occurs to post-transcriptionally upregulate *MECP2*. *MECP2* transcripts are stabilized by the absence of the pluripotency-specific stem cell miRNAs, and the neuron-specific protein HuC outcompetes TIA1 in order to enhance ribosome engagement. The overall effect is that, although active transcription rates for *MECP2* are similar in hESCs and neurons, post-transcriptional mechanisms ensure that MECP2 protein accumulates to high levels only in neurons. Still, the precise role of PUM1 in neurons is unclear. Further analysis is required to fully test the functional significance of the entire 3' UTR sequence.

MECP2 mRNA Destabilization by PUM1 and miRNAs in hESCs

We found that active nascent transcription of *MECP2* is essentially the same between hESCs and neurons. Tellingly, hESCs accumulate primarily the short 3′ UTR isoform, while the level of the long 3′ UTR isoform progressively increases during neurodevelopment. The most functionally significant region of the 3′ UTR involved in mRNA stability was mapped to the conserved PBE2-binding site and its interactions with PUM1. Moreover, the nearby seed sequences for the pluripotency-associated miRNAs hsa-miR-200a and hsa-miR-302c act in concert with, but do not require, PUM1 for this function. Our results implicate *MECP2* as a target of the pluripotency-specific miR-200a and miR-302c in hESCs. These miRNAs are known to regulate genes via mRNA decay, and they have been used to promote somatic cell reprogramming (Judson et al., 2009), which should downregulate MECP2 in the resulting iPSCs.

We found that *PUM1* overexpression reduced MECP2 protein levels in hESC-derived neurons, and this was accompanied by reduced dendrite complexity and smaller soma size. PUM1 regulates *ATAXIN1* mRNA levels in the mouse brain causing a Spinocerebellar ataxia type 1 (SCA1)-like neurodegeneration phenotype (Gennarino et al., 2015). Our data expand on the importance of PUM1 as a key post-transcriptional regulator of neurodevelopment and proper maintenance of neuronal morphology, and they implicate *MECP2* as a PUM1 target. Its role in degrading the *MECP2* long 3′ UTR in hESCs supports a different viewpoint for the use of APA sites in post-transcriptional control of neuronal genes. Indeed, a general observation is that many transcripts associated with neuronal functions undergo 3′ UTR lengthening during neurodevelopment (Miura et al., 2013). Our results suggest that this lengthening is not necessarily related to tissue-specific changes in PA site usage, but instead these long 3′ UTRs may be constitutively transcribed and become targets for mRNA degradation in precursor cell types.

MECP2 Translational Control by TIA1 and HuC RBPs

We elucidated a previously unappreciated translational regulatory mechanism controlling MECP2 protein levels during neurodevelopment. Our polysome association and western blot data suggest that translation of *MECP2* dramatically increases during differentiation from hESCs to neurons. The most functionally significant region of the 3′ UTR involved in translational efficiency was a U-rich sequence element immediately upstream of the first PA site. This element is present in all APA *MECP2* transcript variants, and it mediates the switch from translational repression in hESCs to translation enhancement in neurons. The ability of the same sequence element to confer such strikingly opposite effects on translation is dependent on TIA1 and HuC, which have been reported to compete for the same U-rich element in human cells (Zhu et al., 2006). We found that TIA1 is responsible for translational repression of *MECP2* transcripts in hESCs, consistent with the known function of TIA1 that segregates targeted mRNAs from actively translating polysomes (López de Silanes et al., 2005). Moreover, an interesting feature of translational

Figure 7. Translation of *MECP2* Transcripts Is Silenced in hESCs and Enhanced in Neurons

(A) qRT-PCR from polysome profiles of total RNA from hESCs and neurons. mRNA levels were normalized by spike-in RNAs and plotted as a percentage of total. *ACTB* mRNA levels were used as a positive control of active translation in both cells (n = 3). Error bars, SEM.

(B) Luciferase activity and mRNA levels of hESCs and neurons transfected with plasmids harboring WT or mutant U-rich element present in the 1–149 region (n = 3) are shown.

(C) Luciferase activity in hESCs using plasmids harboring WT or mutant U-rich element and knockdown of TIA1 (n = 3) are shown. Error bars, SEM; *p < 0.05 (ANOVA, Bonferroni post-test).

(D) Western blot and quantification of MECP2 protein levels after knockdown of TIA1 in hESCs (n = 3) are shown. Error bars, SEM; *p < 0.05 (Student's t test).

(E and F) Confocal imaging (E) and quantification (F) of RNA-FISH using probes for *MECP2* total and long transcripts and TIA1 immunostaining in hESC are shown.

(G) TIA1 antibody specificity demonstrated by confocal imaging of immunostained hESC after knockdowns. Scale bars, 5 μm (E, low magnification), 2.5 μm (E, high magnification), and 10 μm (G, low magnification).

(H) Luciferase assay in neurons using plasmids harboring WT or mutant U-rich element and HuC knockdowns are shown.

(I and J) Western blot (I) and quantification (J) of MECP2 protein levels after HuC overexpression in hESC-derived neurons (n = 3). Error bars, SEM; *p < 0.05 and ***p < 0.005 (Student's t test). See also Figure S7.

silencing promoted by TIA1 is its association with translation initiation factors, which can promptly re-engage translation of the targeted mRNAs upon proper environmental cues (Kedersha et al., 2002). Thus, it is likely that TIA1 keeps the pool of developmentally associated transcripts, such as *MECP2*, translationally silenced in pluripotent cells and early stages of development. We also found that translation enhancement of *MECP2* in neurons is dependent on HuC protein, potentially enhancing translation of both short and long *MECP2* transcript isoforms.

Our findings provide extensive insight into the post-transcriptional regulation of *MECP2* in hESCs and neurons, and they have implications for neurodevelopment. Many mutations have been reported in the long 3′ UTR (Coutinho et al., 2007), and, conceivably, these may affect the post-transcriptional circuitry and contribute to abnormal neuronal function. Thus, it may prove critical for gene therapy to incorporate functional 3′ UTR motifs into gene transfer vectors to deliver physiological levels of MECP2 in affected cell types.

EXPERIMENTAL PROCEDURES

Cell Culture and Cortical Neuronal Differentiation

H9 hESCs obtained from the National Stem Cell Bank (WiCell) and Rett syndrome iPSCs (Cheung et al., 2011) were cultured with mTeSR1 culture medium (STEMCELL Technologies) on Becton Dickinson hESC-qualified matrigel. Pluripotent stem cell work was approved by the Canadian Institutes of Health Research Stem Cell Oversight Committee and The Hospital for Sick Children Research Ethics Board. An embryoid body (EB)-based method was used for neuronal induction of NPCs (Brennand et al., 2011). See the Supplemental Experimental Procedures for details. The 293T cells were cultured in DMEM with 10% fetal bovine serum (Invitrogen).

Total RNA Extraction, qRT-PCR, and mRNA Half-Life Assay

Total RNA was processed using RNeasy Plus kit (QIAGEN) and SuperScript III reverse transcriptase (Invitrogen) with random hexamer primers. For the qRT-PCR, we used SYBR Select PCR Master Mix (Applied Biosystems) with Glyceraldehyde 3-phosphate dehydrogenase (GAPDH) or 18S as internal amplification controls. Fold changes were calculated by the $2^{-(\Delta\Delta Ct)}$ method. For half-life assays, 10 μg/mL actinomycin D (Sigma-Aldrich) was added to hESCs, neurons, or 293T cells. RNAs were isolated at the indicated time points for qRT-PCR.

Nascent Transcription Assay

The hESCs and 3-week-old neurons were incubated with 0.5 μM EU (Invitrogen) for 30 min. Total RNA was extracted and processed using Click-iT Nascent RNA Capture kit (Invitrogen) according to the manufacturer's instructions. The captured RNAs were used as a template for cDNA synthesis followed by qRT-PCR.

miRNA Overexpression and Knockdown

For miRNA overexpression, 293T cells or hESCs were grown overnight and transfected with mirVana mimics-miRNA (Invitrogen) as follows: hsa-miR-200a-3p (MC10991), hsa-miR-302c-5p (MC10531), and mimic negative control 1. For miRNA knockdown, cell were transfected with anti-miR-200a-3p (MH 105991), anti-miR-302c-5p (MH 10531), or anti-miR-Mimic control 1 (Invitrogen). All transfections were carried out using Lipofectamine RNAiMAX (Invitrogen) and RNA was collected after 48 hr.

RIP qRT-PCR

The hESCs were seeded in two 10-cm dishes and grown overnight. Cells were then washed in ice-cold PBS. RIPs were carried out using EZ-Magna RIP-RNA Immunoprecipitation kit (Millipore) according to the manufacturer's instructions. 5 μg of antibodies anti-TIA1, anti-PUM1, and anti-HuC were used per reaction (see the Supplemental Experimental Procedures); 5 μg of each isotype IgG antibody was used as a negative control. Target transcripts were detected by qRT-PCR and plotted as percentage of input.

RNA-FISH

RNA-FISH was performed using RNAscope kit (Advanced Cell Diagnostics). Probes targeting the full length of *MECP2* coding sequence (CDS) or the long 3′ UTR sequence of *MECP2* mRNA (5,000–8,554 nt counted from first nucleotide of the 3′ UTR) and negative control *DapB* were designed using Advanced Cell Diagnostics's (ACD's) proprietary algorithm. In brief, hESCs cultured for 5 days were fixed with 4% paraformaldehyde (PFA) and dehydrated with ethanol, followed by cell pretreatment, probe hybridization, and signal amplification according to the manufacturer's instructions. Cells were then immunostained for PUM1 or TIA1. The z stacks of images of random regions were taken with an optical slice thickness of 0.1 μm, using a 60× objective on an Olympus IX81 fluorescence microscope equipped with a Hamamatsu C9100-13 back-thinned electron multiplying charged coupled device (EM-CCD) camera and Okogawa CSU X1 spinning-disk confocal scan head. For quantification, mRNA foci were identified as bright punctate dots present in the nucleus and/or cytoplasm, and about 30–60 cells were quantified in each condition. The mRNA foci that were fully or partially overlapped with PUM1-positive or TIA1-positive granules from z stacked images were counted.

Statistical Analysis

All results presented are the average of at least three experiments expressed as mean ± SEM. Statistical significance was determined by two-way ANOVA with Bonferroni post hoc analyses or Student's unpaired t test, as indicated in the figure legends, using Prism 5 (GraphPad). Probabilities of $p < 0.05$ were considered significant.

SUPPLEMENTAL INFORMATION

Supplemental Information includes Supplemental Experimental Procedures, seven figures, and one table and can be found with this article online at http://dx.doi.org/10.1016/j.celrep.2016.09.049.

AUTHOR CONTRIBUTIONS

Conceptualization, D.C.R. and J.E.; Methodology, D.C.R., D.-S.K., and J.E.; Investigation, D.C.R., D.-S.K., G.Y., K.Z., K.C.H.H., R.S.F.M., P.J.R., M.Z., A.P., and W.W.; Software, K.C.H.H. and Q.M.; Writing – Original Draft, D.C.R., D.-S.K., G.Y., K.C.H.H., and J.E.; Writing – Review & Editing, D.C.R., D.-S.K., G.Y., K.Z., K.C.H.H., R.S.F.M., P.J.R., M.Z., A.P., W.W., B.J.B., Q.M., and J.E.; Visualization, D.C.R., G.Y., and K.C.H.H.; Funding Acquisition, B.J.B., J.E.; Supervision, B.J.B., Q.M., and J.E.

ACKNOWLEDGMENTS

We thank Johanna Rommens and Holly Liu for polysome-profiling resources; Freda Miller for RNA-FISH resources; the SickKids Imaging, SickKids Proteomics, Analytics Robotics & Chemical Biology Centre (SPARC), and The Centre for Applied Genomics (TCAG) Facilities for services; and Tadeo Thompson and Peter Pasceri for technical assistance. The research was supported by Canadian Institutes of Health Research (CIHR) grants (to B.J.B.; MOP-133423 and EPS-129129 to J.E.), the Ontario Brain Institute (POND network to J.E.), and the National Research Foundation, Korea (NRF-2015R1D1A1A01056649 to D.-S.K.). D.C.R. was supported by a RettSyndrome.org Mentored Fellowship and SickKids Restracomp Fellowship, D.-S.K. by a National Research Foundation of Korea Fellowship award, P.J.R. by an Ontario Stem Cell Initiative Fellowship, K.Z. by a CIHR Vanier Canada Graduate Studentship, G.Y. by Brain Canada Mental Health Fellowship, and K.H. by Ontario Graduate Scholarship and CIHR Banting and Best Doctoral Research Award.

Received: December 17, 2015
Revised: August 5, 2016
Accepted: September 15, 2016
Published: October 11, 2016

REFERENCES

Brennand, K.J., Simone, A., Jou, J., Gelboin-Burkhart, C., Tran, N., Sangar, S., Li, Y., Mu, Y., Chen, G., Yu, D., et al. (2011). Modelling schizophrenia using human induced pluripotent stem cells. Nature *473*, 221–225.

Chahrour, M., and Zoghbi, H.Y. (2007). The story of Rett syndrome: from clinic to neurobiology. Neuron *56*, 422–437.

Cheung, A.Y.L., Horvath, L.M., Grafodatskaya, D., Pasceri, P., Weksberg, R., Hotta, A., Carrel, L., and Ellis, J. (2011). Isolation of MECP2-null Rett Syndrome patient hiPS cells and isogenic controls through X-chromosome inactivation. Hum. Mol. Genet. *20*, 2103–2115.

Coutinho, A.M., Oliveira, G., Katz, C., Feng, J., Yan, J., Yang, C., Marques, C., Ataíde, A., Miguel, T.S., Borges, L., et al. (2007). MECP2 coding sequence and 3'UTR variation in 172 unrelated autistic patients. Am. J. Med. Genet. B. Neuropsychiatr. Genet. *144B*, 475–483.

Gennarino, V.A., Singh, R.K., White, J.J., De Maio, A., Han, K., Kim, J.-Y., Jafar-Nejad, P., di Ronza, A., Kang, H., Sayegh, L.S., et al. (2015). Pumilio1 haploinsufficiency leads to SCA1-like neurodegeneration by increasing wild-type Ataxin1 levels. Cell *160*, 1087–1098.

Goldstrohm, A.C., Seay, D.J., Hook, B.A., and Wickens, M. (2007). PUF protein-mediated deadenylation is catalyzed by Ccr4p. J. Biol. Chem. *282*, 109–114.

Han, K., Gennarino, V.A., Lee, Y., Pang, K., Hashimoto-Torii, K., Choufani, S., Raju, C.S., Oldham, M.C., Weksberg, R., Rakic, P., et al. (2013). Human-specific regulation of MeCP2 levels in fetal brains by microRNA miR-483-5p. Genes Dev. *27*, 485–490.

Hansen, D.V., Rubenstein, J.L.R., and Kriegstein, A.R. (2011). Deriving excitatory neurons of the neocortex from pluripotent stem cells. Neuron *70*, 645–660.

Ince-Dunn, G., Okano, H.J., Jensen, K.B., Park, W.-Y., Zhong, R., Ule, J., Mele, A., Fak, J.J., Yang, C., Zhang, C., et al. (2012). Neuronal Elav-like (Hu) proteins regulate RNA splicing and abundance to control glutamate levels and neuronal excitability. Neuron *75*, 1067–1080.

Jao, C.Y., and Salic, A. (2008). Exploring RNA transcription and turnover in vivo by using click chemistry. Proc. Natl. Acad. Sci. USA *105*, 15779–15784.

Judson, R.L., Babiarz, J.E., Venere, M., and Blelloch, R. (2009). Embryonic stem cell-specific microRNAs promote induced pluripotency. Nat. Biotechnol. *27*, 459–461.

Kedde, M., van Kouwenhove, M., Zwart, W., Oude Vrielink, J.A.F., Elkon, R., and Agami, R. (2010). A Pumilio-induced RNA structure switch in p27-3′ UTR controls miR-221 and miR-222 accessibility. Nat. Cell Biol. *12*, 1014–1020.

Kedersha, N., Chen, S., Gilks, N., Li, W., Miller, I.J., Stahl, J., and Anderson, P. (2002). Evidence that ternary complex (eIF2-GTP-tRNA(i)(Met))-deficient preinitiation complexes are core constituents of mammalian stress granules. Mol. Biol. Cell *13*, 195–210.

Klein, M.E., Lioy, D.T., Ma, L., Impey, S., Mandel, G., and Goodman, R.H. (2007). Homeostatic regulation of MeCP2 expression by a CREB-induced microRNA. Nat. Neurosci. *10*, 1513–1514.

Kriaucionis, S., and Bird, A. (2004). The major form of MeCP2 has a novel N-terminus generated by alternative splicing. Nucleic Acids Res. *32*, 1818–1823.

Li, Y., Wang, H., Muffat, J., Cheng, A.W., Orlando, D.A., Lovén, J., Kwok, S.-M., Feldman, D.A., Bateup, H.S., Gao, Q., et al. (2013). Global transcriptional and translational repression in human-embryonic-stem-cell-derived Rett syndrome neurons. Cell Stem Cell *13*, 446–458.

López de Silanes, I., Galbán, S., Martindale, J.L., Yang, X., Mazan-Mamczarz, K., Indig, F.E., Falco, G., Zhan, M., and Gorospe, M. (2005). Identification and functional outcome of mRNAs associated with RNA-binding protein TIA-1. Mol. Cell. Biol. *25*, 9520–9531.

Lyst, M.J., and Bird, A. (2015). Rett syndrome: a complex disorder with simple roots. Nat. Rev. Genet. *16*, 261–275.

Maroof, A.M., Keros, S., Tyson, J.A., Ying, S.-W., Ganat, Y.M., Merkle, F.T., Liu, B., Goulburn, A., Stanley, E.G., Elefanty, A.G., et al. (2013). Directed differentiation and functional maturation of cortical interneurons from human embryonic stem cells. Cell Stem Cell *12*, 559–572.

Menendez, L., Yatskievych, T.A., Antin, P.B., and Dalton, S. (2011). Wnt signaling and a Smad pathway blockade direct the differentiation of human pluripotent stem cells to multipotent neural crest cells. Proc. Natl. Acad. Sci. USA *108*, 19240–19245.

Miles, W.O., Tschöp, K., Herr, A., Ji, J.-Y., and Dyson, N.J. (2012). Pumilio facilitates miRNA regulation of the E2F3 oncogene. Genes Dev. *26*, 356–368.

Miura, P., Shenker, S., Andreu-Agullo, C., Westholm, J.O., and Lai, E.C. (2013). Widespread and extensive lengthening of 3′ UTRs in the mammalian brain. Genome Res. *23*, 812–825.

Nicoleau, C., Varela, C., Bonnefond, C., Maury, Y., Bugi, A., Aubry, L., Viegas, P., Bourgois-Rocha, F., Peschanski, M., and Perrier, A.L. (2013). Embryonic stem cells neural differentiation qualifies the role of Wnt/β-Catenin signals in human telencephalic specification and regionalization. Stem Cells *31*, 1763–1774.

Parker, R., and Sheth, U. (2007). P bodies and the control of mRNA translation and degradation. Mol. Cell *25*, 635–646.

Pelka, G.J., Watson, C.M., Christodoulou, J., and Tam, P.P.L. (2005). Distinct expression profiles of Mecp2 transcripts with different lengths of 3'UTR in the brain and visceral organs during mouse development. Genomics *85*, 441–452.

Peng, C., Li, N., Ng, Y.-K., Zhang, J., Meier, F., Theis, F.J., Merkenschlager, M., Chen, W., Wurst, W., and Prakash, N. (2012). A unilateral negative feedback loop between miR-200 microRNAs and Sox2/E2F3 controls neural progenitor cell-cycle exit and differentiation. J. Neurosci. *32*, 13292–13308.

Shahbazian, M.D., Antalffy, B., Armstrong, D.L., and Zoghbi, H.Y. (2002). Insight into Rett syndrome: MeCP2 levels display tissue- and cell-specific differences and correlate with neuronal maturation. Hum. Mol. Genet. *11*, 115–124.

Simone, L.E., and Keene, J.D. (2013). Mechanisms coordinating ELAV/Hu mRNA regulons. Curr. Opin. Genet. Dev. *23*, 35–43.

Singh, J., Saxena, A., Christodoulou, J., and Ravine, D. (2008). MECP2 genomic structure and function: insights from ENCODE. Nucleic Acids Res. *36*, 6035–6047.

van de Leemput, J., Boles, N.C., Kiehl, T.R., Corneo, B., Lederman, P., Menon, V., Lee, C., Martinez, R.A., Levi, B.P., Thompson, C.L., et al. (2014). CORTECON: a temporal transcriptome analysis of in vitro human cerebral cortex development from human embryonic stem cells. Neuron *83*, 51–68.

Van Etten, J., Schagat, T.L., Hrit, J., Weidmann, C.A., Brumbaugh, J., Coon, J.J., and Goldstrohm, A.C. (2012). Human Pumilio proteins recruit multiple deadenylases to efficiently repress messenger RNAs. J. Biol. Chem. *287*, 36370–36383.

Yokoshi, M., Li, Q., Yamamoto, M., Okada, H., Suzuki, Y., and Kawahara, Y. (2014). Direct binding of Ataxin-2 to distinct elements in 3′ UTRs promotes mRNA stability and protein expression. Mol. Cell *55*, 186–198.

Zhu, H., Hasman, R.A., Barron, V.A., Luo, G., and Lou, H. (2006). A nuclear function of Hu proteins as neuron-specific alternative RNA processing regulators. Mol. Biol. Cell *17*, 5105–5114.